Near Surface Damage and Mixing in Si-Cl_2-Ar Atomic Layer Etching Processes: Insights from Molecular Dynamics Simulations

Joseph R. Vella[†] and David B. Graves[*,‡]

†Princeton Plasma Physics Laboratory, Princeton, NJ 08540 USA

‡Princeton Plasma Physics Laboratory, Princeton, NJ 08540 USA and Department of Chemical and Biological Engineering,Princeton University, Princeton, NJ 08540 USA

E-mail: dgraves@pppl.gov

March 24, 2023

Abstract

Silicon-chlorine-argon (Si-Cl_2-Ar) atomic layer etching (ALE) is simulated using classical molecular dynamics (MD). The simulations provide a detailed view into the the near surface region during ALE processing. Bombardment of Ar^+ ions creates a mixed amorphous region that significantly differs from the picture of ideal ALE. There is also a significant change in Si etch yield and etch product distribution as a function of Ar^+ ion fluence. The Si etch yield is highest at the beginning of the bombardment step but eventually decays to the physical sputtering yield. Atomic Cl and silicon chlorides are major etch products at the start of ion bombardment step, but quickly decay. Atomic Si yields remain relatively constant as a function of Ar^+ ion fluence. A new schematic of Si-Cl_2-Ar ALE is presented in order to emphasize the complex behavior observed in MD simulations.

I. Introduction

The continual reduction of critical dimensions in semiconductor devices demands etching processes that can achieve, or at least approach, atomic-level fidelity in a manufacturing setting. Plasma-assisted atomic layer etching (ALE) processes, currently used in industry, show promise in achieving controlled removal of substrate material with atomic layer precision.[1–8] ALE consists of two ideally self-limiting sub-steps that are separated in space or time. The first step is the chemical modification of the top layer of atoms on the substrate in order to weaken the bonds to the underlying atoms. The second step is the removal of the modified layer with inert ions. Perhaps the the most well-known example is silicon (Si) ALE using chlorine (Cl) (gas or plasma) for the first step and argon (Ar^+) ions for the second step. A schematic of the ideal process of Si-Cl_2-Ar ALE (which has been studied extensively in the literature experimentally[9–16]) is given as Figure 1. We refer to this as an "ideal" ALE

process because only one layer of Si is removed and no damage is done to the underlying crystal structure.

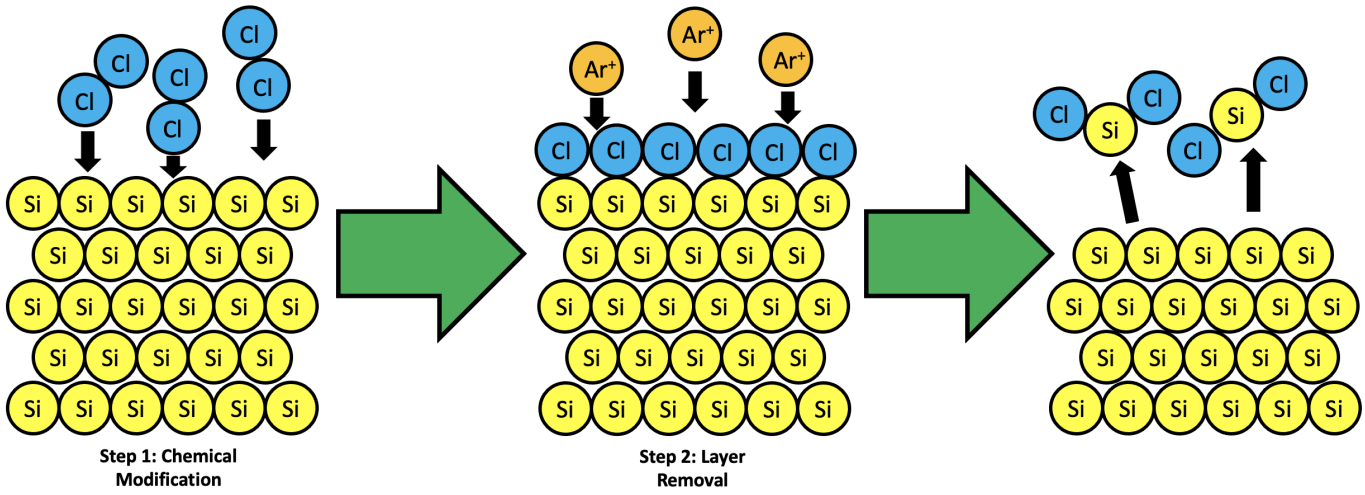

Figure 1: Illustration of an ideal Si-Cl_2-Ar ALE process.

However, at the atomic scale, this schematic does not represent an accurate illustration of plasma-assisted ALE. For example, it is known that ion bombardment of Si surfaces induces some degree of near-surface mixing of the underlying crystal structure and creates an amorphous layer.[17–29] The near-surface crystal structure will inevitably be disturbed when exposed to energetic ions with energies above about 10 eV. Furthermore, when ion bombardment is considered in the context of ALE (where the ions are preceded by a chemical modification step) molecular dynamics (MD) simulations show the chemical modification species can be mixed into the amorphous layer of Si.[30,31] Previous work using a Monte Carlo Feature Profile model (MCFPM) to examine Si ALE have also considered this mixed layer.[32] These phenomena can have profound implications for a truly mechanistic understanding of ALE.

In some ways, ALE simplifies plasma etch processes by separating the "chemical" component of surface modification in an initial step from the "physical" component of etch product removal in a subsequent step. But in other ways, ALE introduces additional complexities because it causes changes in the near-surface region that vary in both time and depth.

Further, even for a relatively simple ALE protocol that involves a molecular gas exposure, rather than plasma, in the surface modification step, there is still a large set of process choices for the second step. Even ignoring various process non-idealities such as species desorbing from and adsorbing to chamber walls, the removal step could be run with a wide range of ion fluxes, exposure times, and ion energies. All of these process choices will in general affect the results, with corresponding differences in the time and depth dependent changes in near-surface composition and structure.

The wide range of process choices makes general conclusions difficult. We focus here on a relatively simple case of Cl_2 gas exposure to modify a silicon surface followed by Ar^+ exposure of the modified layer. In particular, we highlight here the critically important formation of a mixed, amorphized Si layer resulting from ion-induced subsurface mixing. ALE results need to be interpreted in terms of this mixed layer and its variation during the cycle.

The intrinsically transient nature of the process is a second key element. The near surface layer changes continuously during the ion bombardment step. The ion bombardment induced mixed $SiCl_x$ layer shows a continuous reduction of Cl content during the ion bombardment step. This drop in Cl content results in a corresponding drop in Si etch yield.

In this work, we utilize classical MD simulations in order to develop a detailed understanding of Si-Cl_2-Ar ALE. This is done because it is known that MD models explicitly show the formation of Si amorphous layer and subsequent Cl mixing into the layer during ALE simulations. The paper will be organized as follows. Section II will present details of the MD simulations. Section III discusses results. Finally, Section IV will give concluding remarks.

II. Methodology

Simulation Details

Classical MD simulations are performed in order to mimic Si ALE by exposure to Cl_2 gas and Ar^+ ions. The Si-Si, Si-Cl, and Cl-Cl interactions are described using the reactive

empirical bond order (REBO) potential[33] used in the recent work by Vella and Graves.[34] We note that in this version of the potential, the parameters used for Si-Si and Cl-Cl interactions are identical to those developed by Humbird and Graves.[35] However, some Si-Cl parameters were modified to give better agreement with experimental data as described by Vella and Graves.[34] All interactions with Ar^+ ions are described by the Molière potential.[36]

ALE simulations are comprised of successive "impact simulations" where incoming species (either Cl_2 molecules or Ar^+ ions) are placed in a random position above a Si slab. The incoming species is assigned a velocity based on whether they are described as "thermal" or "energetic". "Thermal" species have their x, y, and z components of velocity assigned based on the Maxwell-Boltzmann distribution at 300 K. Only species with a negative z component to their velocity are considered to ensure the incoming species hits the Si surface. On the other hand, "energetic" species only have a negative z component to their velocity, corresponding to a specified energy. Each impact is modeled as a microcanonical (constant number of atoms, constant volume, and constant energy) MD trajectory lasting approximately 2 picoseconds. The Si slab is composed of a 32.60 Å by 32.60 Å by 52.98 Å semi-infinite diamond cubic crystalline structure with periodic boundary conditions imposed in the x and y directions. For a Si slab of this size, one monolayer corresponds to 72 atoms. The top of the slab exposes the (100) crystal facet to a vacuum space. The atoms in the bottom two Si layers are fixed in order to prevent the movement of the slab in the negative z direction. If two monolayers of Si are etched during the course of the ALE simulations, the previously fixed atoms are allowed to move and a new set of fixed atoms are added to the bottom of the layer. This is done in order to prevent the depletion of all Si atoms and keep the Si slab thick enough so that incoming species do not interact with the fixed layers. It should be noted that each time the Si slab is hit with an atom or an ion, the temperature will increase. Therefore, in order to prevent the simulation cell from heating up, a Beredensen thermostat[37] is applied between each impact simulation. In this work, the target temperature for the thermostat is always 300 K. At the end of each impact simulations, a routine is

run in order to identify etch products and remove them from the simulation. More details on the application of the thermostat and the etch product identification routine are given by Humbird[38] as well as our previous manuscript.[34]

The ALE cycles are composed of a chlorination step followed by an ion bombardment step. As mentioned previously, the chlorination step is modeled as exposure of the Si slab to "thermal" Cl_2 molecules. The Si surface is exposed to 3000 impacts of Cl_2 molecules. For the cell size used here, this corresponds to a fluence of 2.82×10^{16} Cl_2 molecules/cm^2. The ion removal step is modeled as exposure of the Si slab to 3000 energetic Ar^+ ions. This corresponds to a fluence of 2.82×10^{16} Ar^+/cm^2. Several different ion energies ranging from 15 to 215 eV are considered in the simulations. The angular distribution of the ions is not considered in this work. We subject a given Si slab to several ALE cycles until cyclic steady state is reached. In all cases, nine cycles were enough to achieve this.

III. Results and Discussion

Figure 2 shows the amount of Si etched and Cl uptake as a function of cycle number for three different Si-Cl_2-Ar ALE simulations. The three cases correspond to Ar^+ ion energies of 25, 100, and 215 eV. The amount of Si etched obviously increases with ion energy, while the average Cl uptake follows the opposite trend.

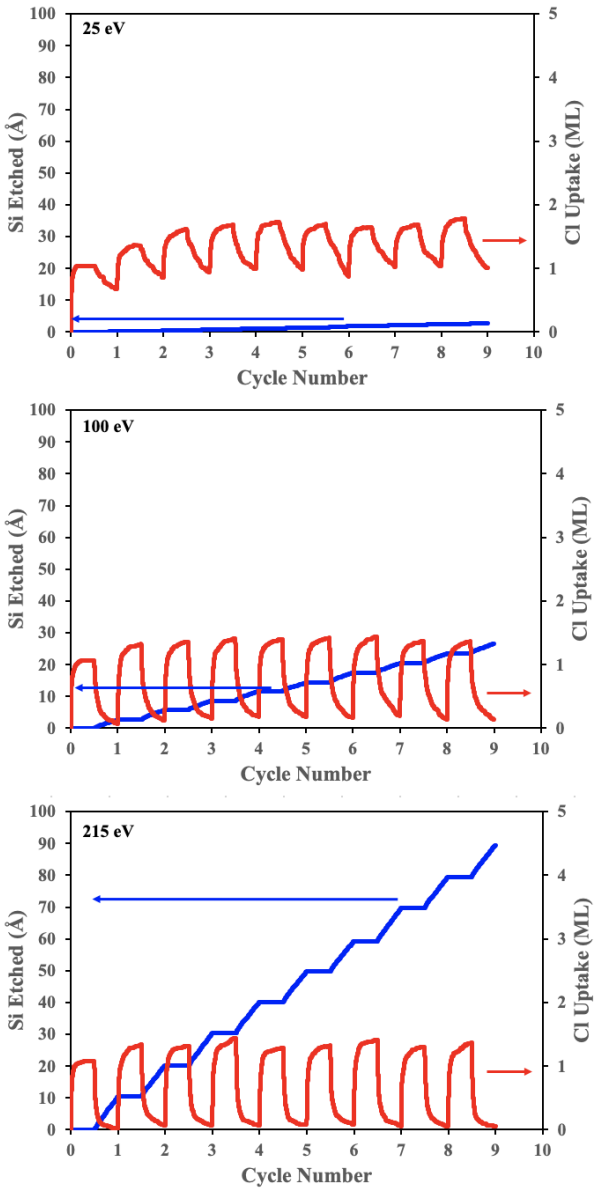

Figure 2: Amount of Si etched (in units of Å) (blue lines) and Cl uptake (in units of equivalent monolayers) (red lines) as a function of cycle number for Si-Cl_2-Ar ALE simulations. One cycle consists of 3000 Cl_2 molecule impacts and 3000 Ar^+ ion impacts. Results are shown for Ar^+ ion energies of 25, 100, and 215 eV.

Figure 3 gives a closer look at the amount of Si etched and Cl uptake during the final cycle of the results given in Figure 2. Note that the units of the x-axis and primary y-axis have changed. The amount of Si etched is now shown in units of equivalent monolayers, and the x-axis is displayed in terms of species impact number (also in units of equivalent

monolayers). This is done in order to better visualize how the Si etch yield evolves during the ion bombardment step. The etch yields are calculated during the first 150 Ar^+ ion impacts (green dash-dotted line) and the final 500 Ar^+ ion impacts (purple dash-dotted line). This is done to study how the etch yield varies with Ar^+ ion fluence.

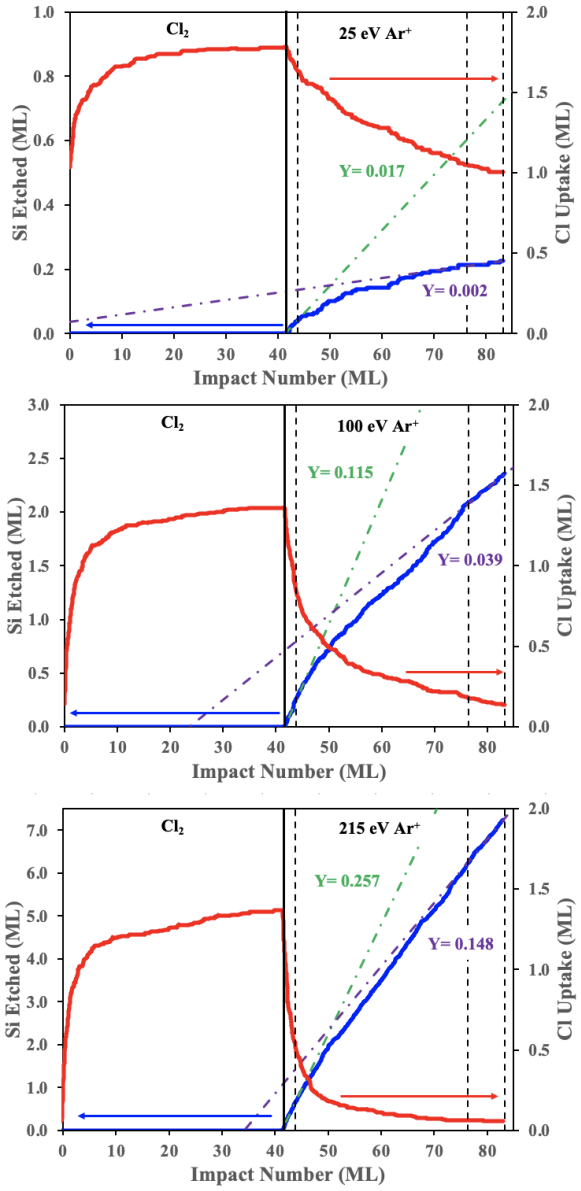

Figure 3: Amount of Si etched (blue lines) and Cl uptake (red lines) as a function of species impact number during the final ALE cycle. All aforementioned quantities are in units of equivalent monolayers. These results correspond to the final cycles shown in Figure 2. Si etch yields are calculated at the beginning of the ion bombardment step (green dash-dotted line) and the end of the ion bombardment step (purple dash-dotted line). Note the different scales of the primary y-axis on each subfigure.

Unsurprisingly the Si etch yield is larger at the beginning of the ion bombardment step, when the Cl concentration is highest. At the beginning of the ion bombardment step the Si etch yield is 0.017, 0.115, and 0.257 for 25 eV, 100 eV, and 215 eV respectively. At the end of

the bombardment step the etch yields are 0.002, 0.039, and 0.148 for 25 eV, 100 eV, and 215 eV respectively. For the 25 eV case, a factor of about 8.5 enhancement in etch yield at the beginning of the bombardment step relative to the end. For the 100 and 215 eV cases, the enhancement factors are roughly 3 and 1.74 respectively. It should be noted that the etch yields seen at the end of the bombardment steps for the 100 and 215 eV cases correspond the physical sputtering of Si by Ar^+ ions. This is because the amount of Cl in the near surface region has been significantly depleted. Figure 4 shows a comparison of the Si etch yield at the beginning of the ion bombardment step (referred to as the "enhanced yield") to the physical sputtering yield, both as a function of the square root of the Ar^+ ion energy. The plot suggests that increase in yield due to the presence of Cl does not monotonically increase with the ion energy. In fact, it appears the largest different between the "enhanced yield" and the physical sputtering yield is around 50 eV.

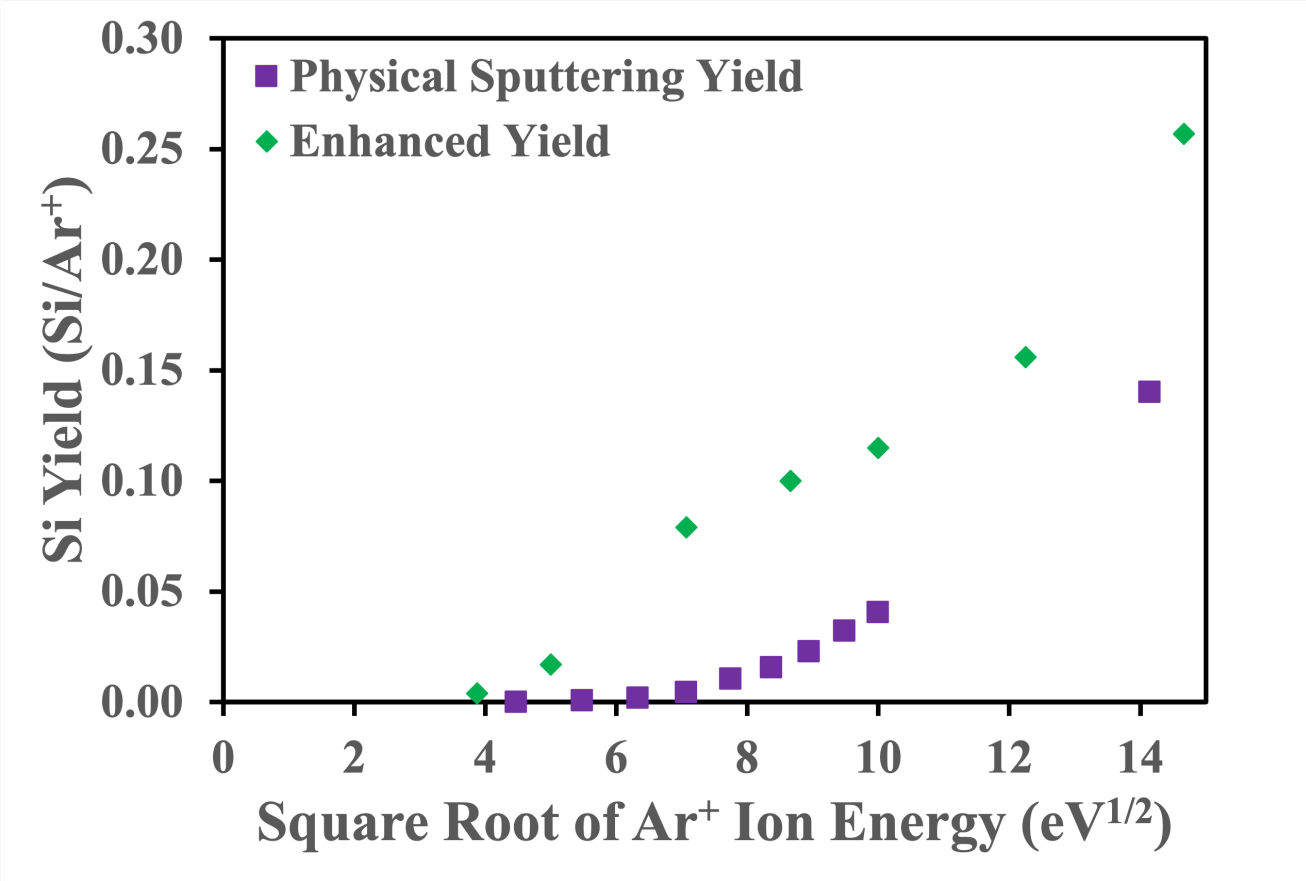

Figure 4: Comparison of the Si physical sputtering yield to the "enhanced Si yield" as a function of the square root of Ar^+ ion energy calculated from MD simulations. The "enhanced Si yield" is the yield seen at the beginning of the ion bombardment step when Cl content is at its maximum, while the physical sputtering yield is the yield with no Cl present.

It is useful to visualize the simulation cell during the course of the final Ar^+ ion bombardment step. Figure 5 shows five snapshots of the simulation cell at various Ar^+ ion fluences for the final ion bombardment step in the 100 eV ALE cycle.

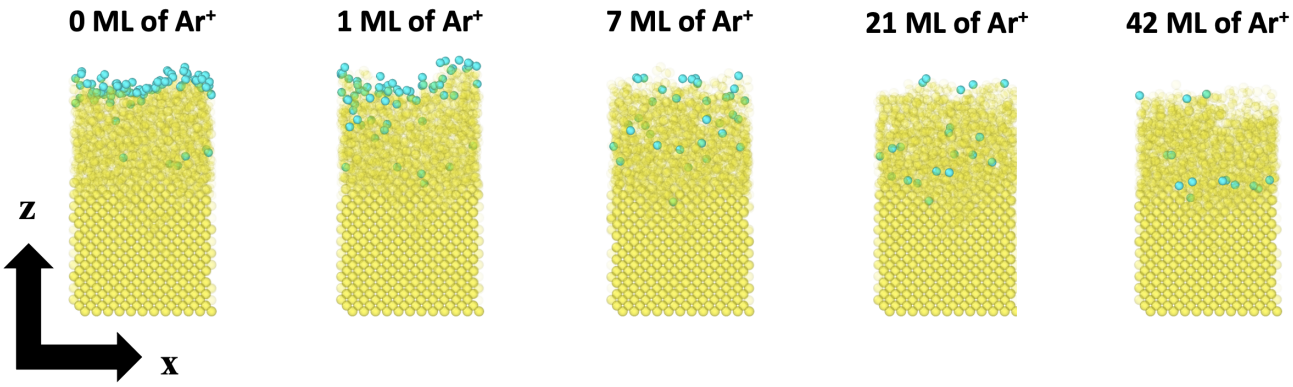

Figure 5: Side views of the simulations cell at various points during the final Ar^+ ion bombardment step. Yellow translucent spheres are Si atoms and cyan spheres are Cl atoms. The Ar^+ ion energy is 100 eV. The near-surface amorphization and Cl mixing is qualitatively different than the ideal ALE illustration in Figure 1. Images were rendered using Ovito.[39]

The first snapshot shows the simulation cell at the very start (0 ML of Ar^+ ion impacts) of the Ar^+ ion bombardment step. Here, we already see a qualitatively different picture of ALE than the ideal case illustrated in Figure 1. The large amount of Cl at the top of the layer is due to the fact that the chlorination step has just ended. Due to the fact this is the final cycle, there is a significant amorphous layer below the Cl layer. There is also some Cl atoms mixed into the amorphous region. In the subsequent snapshots, we see that the Cl layer is depleted, and amorphous mixed region still remains. As mentioned in the introduction, previous studies using MD simulations have also seen this.[30,31] The amount of Cl in the mixed region decreases as the Ar^+ ion dosage increases. The formation of the amorphous layer and the subsequent mixing of Cl into this region causes significant deviation from ideal ALE behavior.

More evidence of this non-ideal behavior is seen by examining the etch products leaving the simulation cell during the ion bombardment step. Figure 6 shows average etch product yields as a function of Ar^+ ion fluence during the final ion bombardment step of the ALE simulations using 80 eV Ar^+ ions. It should be noted that the ALE simulations used to generate this data have a longer ion bombardment step than those previously mentioned (5400 Ar^+ ion impacts as opposed to 3000 Ar^+ ion impacts). This was done in order to

obtain a more complete understanding of how etch product yields evolve as a function of ion fluence.

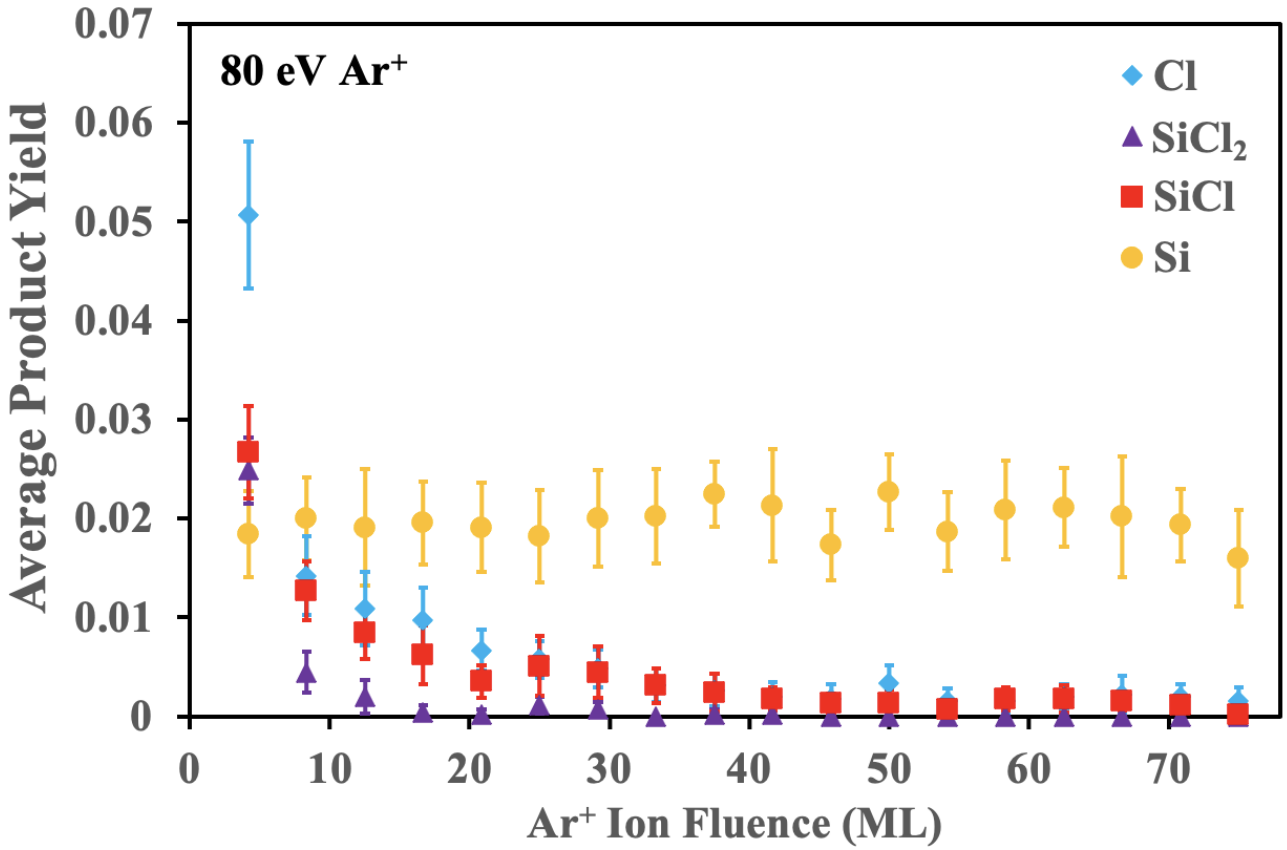

Figure 6: Average product yields as a function of ion fluence (in units of equivalent monolayers). Products are tracked during the final ion bombardment step of an ALE simulation using 80 eV Ar^+ ions. For this case, one ALE cycle consists of 3000 Cl_2 molecule impacts and 5400 Ar^+ ion impacts.

Atomic Cl has the highest etch yield at the beginning of the ion bombardment step, but this quickly decays. This is consistent with the side views shown in Figure 5, that is there is a high concentration of Cl near the top of the surface at the end of the chlorination step. This also agrees with distribution of the etch products studied in our previous work.[31] $SiCl_2$ and SiCl yields follow similar behavior with the former decaying the quickest. Finally the yield for atomic Si remains constant during the entire bombardment step. Moreover, the yield corresponds to the physical sputtering yield at 80 eV (approximately 0.02) for the interatomic potentials used. This value is in good agreement with physical sputtering yield

estimations by Zalm,[40] Monte Carlo simulations utilizing the binary collision approximation,[41] and experimental data.[42]

These findings allow us to form a clearer picture of what is occurring in the near surface region during Si-Cl_2-Ar ALE. As previously stated, the schematic shown as Figure 1 is qualitatively incorrect. The change in the silicon etch yield during the ion bombardment step shown in Figure 3, along with the side views in Figure 5 and the dependence of product yields as a function of ion fluence in Figure 6 forces us to consider a new schematic. This new Si-Cl_2-Ar ALE schematic is given as Figure 7.

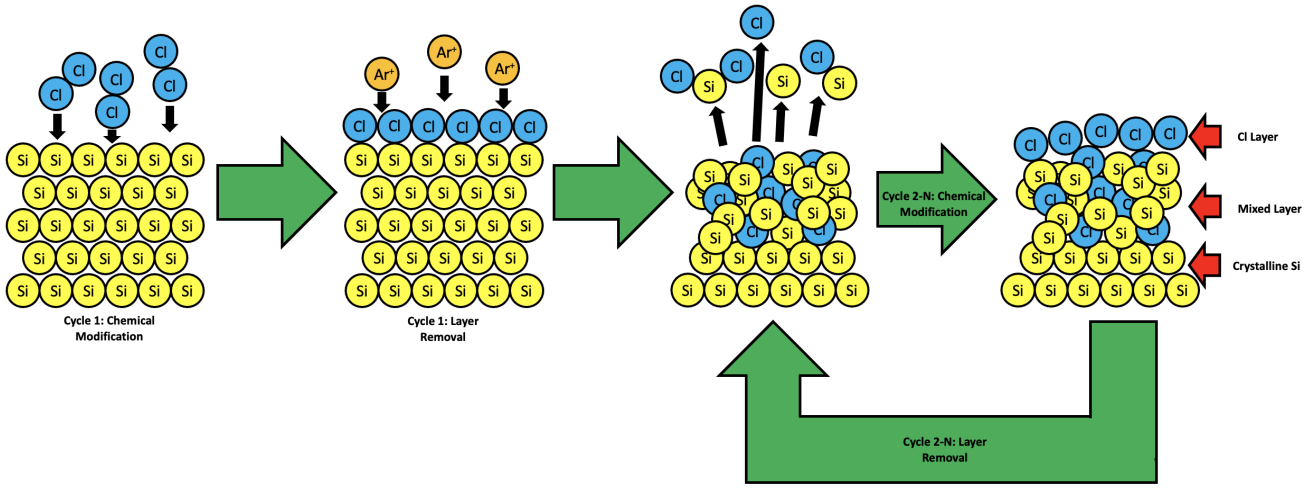

Figure 7: A more realistic schematic of Si-Cl_2-Ar ALE. Note that there is a notable amorphous region formed containing Cl atoms after the initial ion bombardment. Also, a variety of products come off during ion bombardment (atomic Cl, atomic Si, and different silicon chlorides).

Starting from the first illustration, we consider a pristine Si surface being exposed to Cl_2 gas. This is the chlorination step of the first ALE cycle. At this point, we only expect Cl to be at the top of the Si surface. The surface is then subjected to the first ion bombardment step (second illustration). This is where major deviations from the ideal ALE schematic start to occur. The ion bombardment leads to the formation of a mixed amorphous layer as well as etching of atomic Cl, Si, and silicon chlorides (third illustration). Once the ion bombardment step finishes, the next cycle begins, starting with exposure of the surface to

Cl_2 gas once again. The near-surface region after this chlorination step (fourth illustration) looks significantly different than the second illustration due to the mixed amorphous layer. Now, ion bombardment begins again and the near-surface region will look similar to the third illustration. This is why we draw an arrow going from the fourth illustration to the third. Therefore, as more cycles are performed, the near-surface region will alternate between these two illustrations. We note that the schematic does not explicitly deplete the amount of Si atoms present when going from illustration four to illustration three. This is done in order to have a more succinct figure. The interpretation of these illustrations should only be that they represent the atoms near the surface of a Si wafer, not an absolute amount of Si. It should be noted that this schematic shares similarities to Figure 1 in the work by Tinacba et al.[30]

Figure 8 gives a more detailed schematic of the various phenomena occurring at the near surface region during ion bombardment between the third and fourth illustrations. First, note that the Si slab has been divided into three regions (indicated by the red arrows), the Cl layer, the mixed layer, and the crystalline Si region. The green arrows illustrate the various phenomena occurring during the ion bombardment step. These are silicon chloride etching, Si sputtering, Cl sputtering, Cl mixing from the Cl layer into the mixed layer, and Si replenishment from the crystalline regime to the mixed layer. Clearly, the diverse amount of phenomena occurring at the near surface region during ion bombardment creates a much more complex picture of ALE than what is shown in Figure 1.

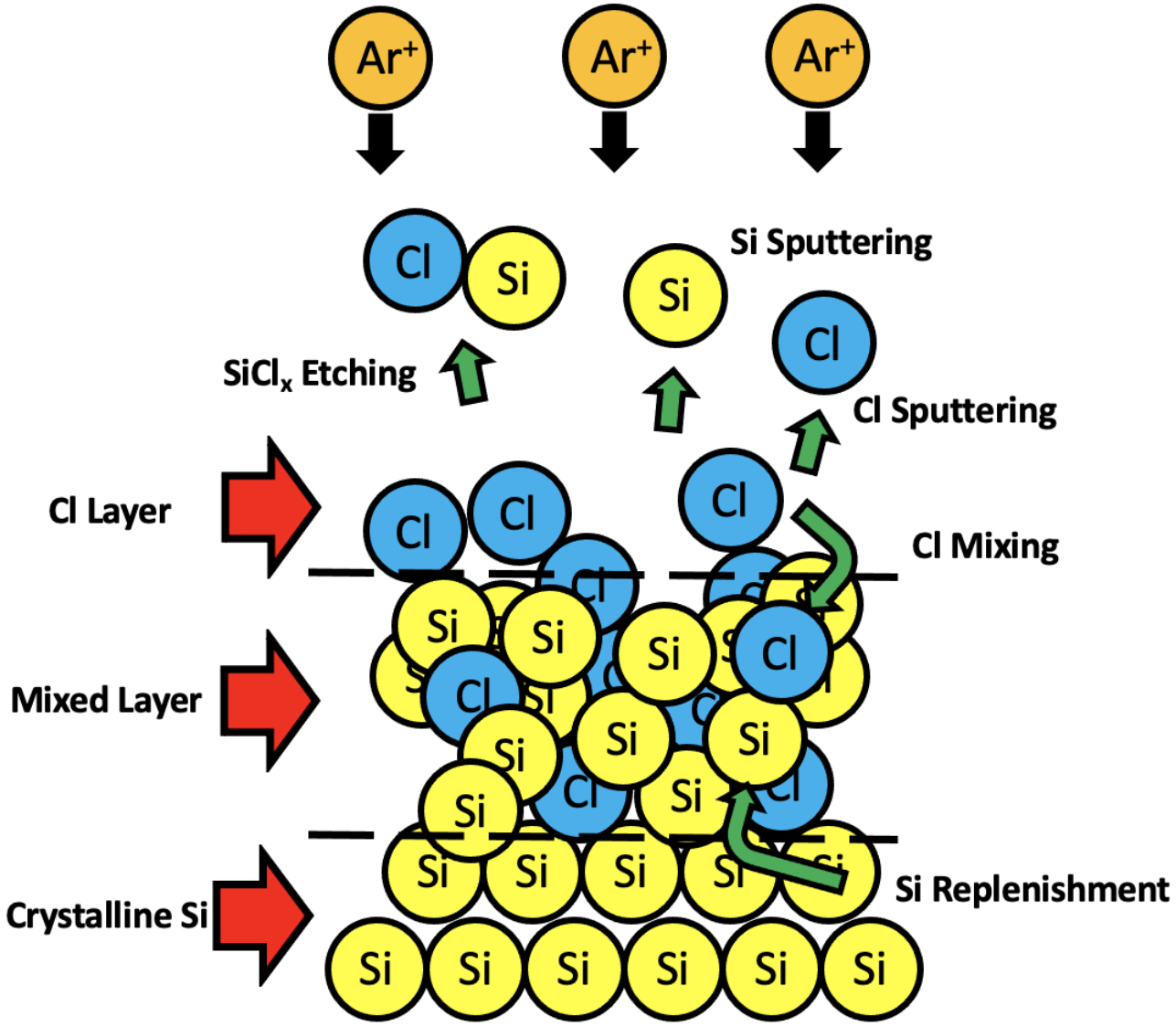

Figure 8: A detailed schematic of what is occurring near the surface of the Si slab during Ar^+ ion bombardment in Si-Cl_2-Ar ALE. Red arrows indicate the different regimes of the near surface region (Cl layer, mixed layer, and crystalline Si region). Green arrows indicate major events that occur in the near surface region during ion bombardment. That is, silicon chloride etching, Si sputtering, Cl sputtering, Cl mixing from the Cl layer into the mixed layer and Si replenishment from the crystalline Si region into the mixed layer.

IV. Concluding Remarks

This paper has presented classical MD simulations of Si-Cl_2-Ar ALE. These simulations were used to build a detailed understanding of the atomic structure of the surface and the etching behavior during an ALE process. The findings help illustrate how the ideal picture of ALE is qualitatively incorrect.

The MD simulations demonstrate how, during the ion bombardment step, the Si etch yield will inevitably decrease as a function of ion fluence. This is because the Cl content in the near surface region also decreases as a function of ion fluence. Side views of the simulation cell explicitly show the presence of an amorphous region with Cl atoms mixed throughout. There is also a significant change in etch product yields over the course of the ion bombardment step. At the beginning of the step, atomic Cl and silicon chlorides dominate the etch product distrbution. The yield of these products quickly decay, while the atomic Si yield remains constant throughout the cycle due to physical sputtering.

It can be concluded that the MD simulations show a more complex picture of the near surface region for even the relatively simple case of Si ALE using Cl_2 gas (as opposed to plasma). There is etching and sputtering of various products from the surface. Cl is mixed into the amorphous region, and Si is replenished to this region from the crystalline regime. Future work will focus on comparing the MD results to experimental data in a rigorous manner. We are particularly interested in looking at etch product yields during Ar^+ ion bombardment. Recent experimental work has been able to monitor etch products of ALE in real time.[43]

Acknowledgements

This work was partially supported by the US Department of Energy OFES,contract # DE-AC02-09CH11466. The authors gratefully acknowledge discussions with Keren Kanarik (Lam Research Corporation), Vince Donnelly (University of Houston), and David Humbird

(DWH Process Consulting).

Author Declarations

Conflict of Interest

The authors have no conflicts to disclose.

Data Availability Statement

The data that support the findings of this study are available from the corresponding author upon reasonable request.

References

(1) Carver, C. T.; Plombon, J. J.; Romero, P. E.; Suri, S.; Tronic, T. A.; Turkot Jr., R. B. Atomic Layer Etching: An Industry Perspective. *ECS J. Solid State Sci. Technol.* **2015**, *4*, N5005–N5009.

(2) Faraz, T.; Roozeboom, F.; Knoops, H. C. M.; Kessels, W. M. M. Atomic Layer Etching: What Can We Learn from Atomic Layer Deposition? *ECS J. Solid State Sci. Technol.* **2015**, *4*, N5023–N5032.

(3) Oehrlein, G. S.; Metzler, D.; Li, C. Atomic Layer Etching at the Tipping Point: An Overview. *ECS J. Solid State Sci. Technol.* **2015**, *4*, N5041–N5053.

(4) Kanarik, K. J.; Lill, T.; Hudson, E. A.; Sriraman, S.; Tan, S.; Marks, J.; Vahedi, V.; Gottscho, R. A. Overview of Atomic Layer Etching in the Semiconductor Industry. *J. Vac. Sci. Technol. A* **2015**, *33*, 020802–1–14.

(5) Chang, J.; Chang, J. P. Achieving Atomistic Control in Materials Processing by Plasma–Surface Interactions. *J. Phys. D: Appl. Phys.* **2017**, *50*, 253001–1–23.

(6) Kanarik, K. J.; Tan, S.; Gottscho, R. A. Atomic Layer Etching: Rethinking the Art of Etch. *J. Phys. Chem. Lett.* **2018**, *9*, 4814–4821.

(7) Arts, K.; Hamaguchi, S.; Ito, T.; Karahashi, K.; Knoops, H. C. M.; Mackus, A. J. M.; Kessels, W. M. M. E. Foundations of Atomic-Level Plasma Processing in Nanoelectronics. *Plasma Sources Sci. Technol.* **2022**, *31*, 103002–1–20.

(8) Kim, D.; Kim, J.; Ahn, D.; Choe, J.; Kim, J.; Jung, E.; Pyo, S. Atomic Layer Etching Applications in Nano-Semiconductor Device Fabrication. *Electron. Mater. Lett.* **2023**, https://doi.org/10.1007/s13391-023-00409-4.

(9) Matsuura, T.; Murota, J.; Sawada, Y.; Ohmi, T. Self-limited Layer-by-Layer Etching of Si by Alternated Chlorine Adsorption and Ar^+ Ion Irradiation. *Appl. Phys. Lett.* **1993**, *63*, 2803–2805.

(10) Suzue, K.; Matsuura, T.; Murota, J.; Sawada, Y.; Ohmi, T. Substrate Orientation Dependence of Self-Limited Atomic-Layer Etching of Si with Chlorine Adsorption and Low-Energy Ar^+ Irradiation. *Appl. Surf. Sci.* **1994**, *82/83*, 422–427.

(11) Kim, B.; Chung, S.; Cho, S. M. Layer-by-Layer Etching of Cl-Adsorbed Silicon Surfaces by Low Energy Ar^+ Ion Irradiation. *Appl. Surf. Sci.* **2002**, *187*, 124–129.

(12) Park, S.; Min, K.; Yoon, B.; Lee, D.; Yeom, G. Precise Depth Control of Silicon Etching Using Chlorine Atomic Layer Etching. *Jpn. J. Appl. Phys.* **2005**, *44*, 389–393.

(13) Park, S.; Lee, D.; Yeom, G. Atomic Layer Etching of Si(100) and Si(111) Using Cl_2 and Ar Neutral Beam. *Electrochem. Solid-State Lett.* **2005**, *8*, C106–C109.

(14) Park, S.; Oh, C.; Lee, D.; Yeom, G. Surface Roughness Variation during Si Atomic

Layer Etching by Chlorine Adsorption Followed by an Ar Neutral Beam Irradiation. *Electrochem. Solid-State Lett.* **2005**, *8*, C177–C179.

(15) Park, S.; Lee, D.; Yeom, G. Atomic Layer Etching of Cl-Adsorbed Silicon by Using a Low-Angle Forward Reflected Ar Neutral Beam. *J. Korean Phys. Soc.* **2005**, *47*, 469–473.

(16) Oh, C.; Park, S.; Lee, H.; Bae, J.; Yeom, G. Surface Analysis of Atomic-Layer-Etched Silicon by Chlorine. *Electrochem. Solid-State Lett.* **2007**, *10*, H94–H97.

(17) Mazey, D. J.; Nelson, R. S.; Barnes, R. S. Observation of Ion Bombardment Damage in Silicon. *Philos. Mag.* **1968**, *17*, 1145–1161.

(18) Morehead, F. F.; Crowder, B. L.; Title, R. S. Formation of Amorphous Silicon by Ion Bombardment as a Function of Ion, Temperature, and Dose. *J. Appl. Phys.* **1972**, *43*, 1112–1118.

(19) Müller, G.; Kalbitzer, S. The Crystalline-to-Amorphous Transition in Ion-Bombarded Silicon. *Philos. Mag. B* **1980**, *41*, 307–325.

(20) Martens, J.; Van Den Bogert, W.; Van Silfhout, A. The influence of Argon Ion Bombardment on the Electrical and Optical Properties of Clean Silicon Surfaces. *Surf. Sci.* **1981**, *105*, 275–288.

(21) Lohner, T.; Mezey, G.; Kótai, E.; Manuaba, A.; Pászti, F.; Dévényi, A.; Gyulai, J. An Investigation of Ion-Bombarded Silicon by Ellipsometry and Channeling Effect. *Nucl. Instrum. Methods Phys. Res.* **1982**, *199*, 405–408.

(22) Lang, B.; Taoufik, A. Critical Energy for Damage at Silicon Surfaces Bombarded with Low-Energy Argon Ions. *Appl. Phys. A* **1986**, *39*, 95–99.

(23) Claverie, A.; Vieu, C.; Fauré, J.; Beauvillain, J. Cross-Sectional High-Resolution Electron Microscopy Investigation of Argon-Ion Implantation-Induced Amorphization of Silicon. *J. Appl. Phys.* **1988**, *64*, 4415–4423.

(24) Winters, H. F.; Coburn, J. W. Surface Science Aspects of Etching Reactions. *Surf. Sci. Rep.* **1992**, *14*, 161–269.

(25) Zhang, X.; Comins, J. D.; Every, A. G.; Stoddart, P. R.; Pang, W.; Derry, T. E. Surface Brillouin Scattering Study of the Surface Excitations in Amorphous Silicon Layers Produced by Ion Bombardment. *Phys. Rev. B* **1998**, *20*, 13677–13685.

(26) Pelaz, L.; Marqués, L. A.; Barbolla, J. Ion-Beam-Induced Amorphization and Recrystallization in Silicon. *J. Appl. Phys.* **2004**, *96*, 5947–5976.

(27) Stevens, A. A. E.; Kessels, W. M. M.; van de Sanden, M. C. M.; Beijerinck, H. C. W. Amorphous Silicon Layer Characteristics During 70-2000 eV Ar^+-ion Bombardment of Si(100). *J. Vac. Sci. Technol. A* **2006**, *24*, 1933–1940.

(28) Humbird, D.; Graves, D. B.; Stevens, A. A. E.; Kessels, W. M. M. Molecular Dynamics Simulations of Ar^+ Bombardment of Si with Comparison to Experiment. *J. Vac. Sci. Technol. A* **2007**, *25*, 1529–1533.

(29) Gebers, P. M.; Gielis, J. J. H.; Beijerinck, H. C. W.; van de Sanden, M. C. M.; Kessels, W. M. M. Amorphous Silicon Layer Characteristics During 70-2000 eV Ar^+-ion Bombardment of Si(100). *J. Vac. Sci. Technol. A* **2010**, *28*, 293–301.

(30) Tinacba, E. J. C.; Isobe, M.; Hamaguchi, S. Surface Damage Formation During Atomic Layer Etching of Silicon with Chlorine Adsorption. *J. Vac. Sci. Technol. A* **2021**, *39*, 042603–1–11.

(31) Vella, J. R.; Humbird, D.; Graves, D. B. Molecular Dynamics Study of Silicon Atomic

Layer Etching by Chlorine Gas and Argon Ions. *J. Vac. Sci. Technol. B* **2022**, *40*, 023205–1–9.

(32) Huard, C. M.; Zhang, Y.; Sriraman, S.; Paterson, A.; Kanarik, K. J.; Kushner, M. J. Atomic Layer Etching of 3D Structures in Silicon: Self-limiting and Nonideal Reactions. *J. Vac. Sci. Technol. A* **2017**, *35*, 031306–1–15.

(33) Brenner, D. W.; Shenderova, O. A.; Harrison, J. A.; Stuart, S. J.; Ni, B.; Sinnott, S. B. A Second-Generation Reactive Empirical Bond Order (REBO) Potential Energy Expression for Hydrocarbons. *J. Phys.: Condens. Matter* **2002**, *14*, 783–802.

(34) Vella, J. R.; Graves, D. B. Modification of a Force Field for Molecular Dynamics Simulations of Silicon Etching by Chlorine Atoms. *J. Vac. Sci. Technol. A* **2022**, *40*, 063203–1–7.

(35) Humbird, D.; Graves, D. B. Improved Interatomic Potentials for Silicon-Fluorine and Silicon-Chlorine. *J. Chem. Phys.* **2004**, *120*, 2405–2412.

(36) Moliére, G. Theorie der Streuung schneller geladener Teilchen I. Einzelstreuung am abgeschirmten Coulomb-Feld. *Z. Naturforschung A* **1947**, *2*, 133–145.

(37) Berendsen, H. J. C.; Postma, J. P. M.; van Gunsteren, W. F.; DiNola, A.; Haak, J. R. Molecular Dynamics Coupling to an External Bath. *J. Chem. Phys.* **1984**, *81*, 3684–3690.

(38) Humbird, D. W. Computational Studies of Plasma-Surface Interactions. Ph.D. thesis, University of California, Berkeley, 2004.

(39) Stukowski, A. Visualization and Analysis of Atomistic Simulation Data with OVITO–the Open Visualization Tool. *Modelling Simul. Mater. Sci. Eng.* **2010**, *18*, 015012–1–7.

(40) Zalm, P. C. Some Useful Yield Estimates for Ion Beam Sputtering and Ion Plating at Low Bombarding Energies. *J. Vac. Sci. Technol. B* **1984**, *2*, 151–152.

(41) Yamamura, Y.; Tawara, H. Energy Dependence of Ion-Induced Sputtering Yields from Monatomic Solids at Normal Incidence. *At. Data Nucl. Data Tables* **1996**, *62*, 149–253.

(42) Oostra, D. J.; van Ingen, R. P.; Haring, A.; de Vries, A. E. Near Thereshold Sputtering of Si and SiO_2 in a Cl_2 Environment. *Appl. Phys. Lett.* **1987**, *50*, 1506–1508.

(43) Hao, Q.; Kim, P.; Nam, S.; Kang, S.; Donnelly, V. M. Real-Time Monitoring of Atomic Layer Etching in Cl_2/Ar Pulsed Gas, Pulsed Power plasmas by Optical Emission Spectroscopy. *J. Vac. Sci. Technol. A* (submitted).